Molecular Dynamics of a Water-Lipid Bilayer Interface

Michael A. Wilson and Andrew Pohorille*

Contribution from the Department of Pharmaceutical Chemistry, University of California, San Francisco, California 94143, and NASA Ames Research Center, Moffett Field, California 94035

Received July 2, 1993®

Abstract: We present results of molecular dynamics simulations of a glycerol 1-monooleate bilayer in water. The total length of analyzed trajectories is 5 ns. The calculated width of the bilayer agrees well with the experimentally measured value. The interior of the membrane is in a highly disordered fluid state. Atomic density profiles, orientational and conformational distribution functions, and order parameters indicate that disorder increases toward the center of the bilayer. Analysis of out-of-plane thermal fluctuations of the bilayer surfaces occurring at the time scale of the present calculations reveals that the distribution of modes agrees with predictions of the capillary wave model. Fluctuations of both bilayer surfaces are uncorrelated, yielding Gaussian distribution of instantaneous widths of the membrane. Fluctuations of the width produce transient thinning defects in the bilayer which occasionally span almost half of the membrane. The leading mechanism of these fluctuations is the orientational and conformational motion of head groups rather than vertical motion of the whole molecules. Water considerably penetrates the head group region of the bilayer but not its hydrocarbon core. The total net excess dipole moment of the interfacial water points toward the aqueous phase, but the water polarization profile is non-monotonic. Both water and head groups significantly contribute to the surface potential across the interface. The calculated sign of the surface potential is in agreement with that from experimental measurements, but the value is markedly overestimated. The structural and electrical properties of the water-bilayer system are discussed in relation to membrane functions, in particular transport of ions and nonelectrolytes across membranes.

I. Introduction

Interfaces between biomembranes and water are ubiquitous components of living cells. A host of essential biological processes take place in the proximity of these interfaces. These include adsorption and transduction of energy, passive and active transport of ions and nutrients, transmission of neural signals, mediation of immune response, and membrane fusion.[1] Properties of water-membrane interfaces play a large role in many phenomena of medical and pharmacological interest. Interactions with and transport across membranes of small molecules are of fundamental importance in relation to drug delivery.[2] In another example, it has been postulated that anesthetic molecules act at the water-membrane interface to produce anesthesia.[3] Further interest in water-membrane interfaces is related to their possible role in protobiological evolution. Bilayer vesicles may have been the earliest protocells, and essential bilayer functions may have evolved at their surfaces.[4]

Biological membranes are complex, multicomponent systems consisting of a wide variety of lipids and membrane proteins. The main structural features of membranes are determined by lipids in a bilayer arrangement whereby polar lipid head groups are exposed to external aqueous environment while hydrocarbon tails form the nonpolar interior. Many properties of biomembranes can be investigated by using model systems consisting only of lipid bilayers. Water on both sides of the membrane is essential for stability of the bilayer structure and, therefore, constitutes an integral part of these systems. In this paper we present results of a molecular dynamics (MD) computer simulation study of one such system, in which the bilayer is built of glycerol 1-monooleate (GMO) molecules. Since GMO head groups are uncharged, this choice allows us to avoid computational complications associated with the presence of counterions. The small surface area occupied by GMO molecules is another advantage, which permits inclusion of a sufficiently large number of GMO molecules in the bilayer so that out-of-plane surface fluctuations can be analyzed. A number of MD investigations treated other water-bilayer systems. In these systems the bilayer was formed by dilauroylphosphatidylethanolamine (DPLE),[5,6] decanoate/decanol mixtures,[7] and mixtures of dilauroylphosphatidylserine with dilauroylphosphatidylcholine molecules.[8] Some other computational studies treated more complex bilayer-protein systems.[9,10] However, those studies required a host of additional approximations beyond those assumed in MD calculations.

The structural characteristics of large biomolecules, such as proteins and nucleic acids, are traditionally discussed in the context of their functions. Similar structure-function relationships also have been proposed for membranes. It has been suggested that thinning defects in the membrane, caused by molecular-scale fluctuations of the surface, provide effective pathways for unassisted ion transport.[11,12] Water penetration into these defects may account for the high permeability of membranes to water and protons.[11,12] The ordering of head groups and water molecules

* Address correspondence to this author at the University of California.

® Abstract published in *Advance ACS Abstracts*, December 1, 1993.

(1) Gennis, R. B. *Biomembranes: Molecular Structure and Function*; Springer-Verlag: New York, 1989.

(2) Guy, R. H.; Honda, D. H. *Int. J. Pharm.* **1984**, *19*, 129-137. Knepp, V. M.; Guy, R. H. *J. Phys. Chem.* **1989**, *93*, 6817-6823 and references herein.

(3) (a) Kamaya, H.; Ueda, I.; Eyering, H. In *Molecular Mechanism of Anesthesia. Progress in Anesthesiology*; Fink, B. R., Ed.; Raven Press: New York, 1980; Vol. 2, pp 429-433. (b) Forrest, B. J.; Mattai, J. *Biochemistry* **1985**, *24*, 7148-7153. (c) Enders, A. *Biochim. Biophys. Acta* **1990**, *1029*, 43-50. (d) Eger, E. I.; Liu, J.; Koblin, D.; Halsey, M.; Chortkoff, B. *Anesthesia* **1993**, in press.

(4) Morowitz, H. J. *Beginnings of Cellular Life*; Yale University Press: New Haven, 1992.

(5) (a) Berkowitz, M. L.; Raghavan, K. *Langmuir* **1991**, *7*, 1042-1044. (b) Raghavan, K.; Reddy, M. R.; Berkowitz, M. L. *Langmuir* **1992**, *8*, 233-240.

(6) Damodaran, K. V.; Merz, K. M.; Garber, B. P. *Biochemistry* **1992**, *31*, 7656-7664.

(7) Egberts, E.; Berendsen, H. J. C. *J. Phys. Chem.* **1988**, *89*, 3718-3732.

(8) Charifson, P. S.; Hiskey, R. G.; Pedersen, L. G. *J. Comput. Chem.* **1990**, *11*, 1181-1186. Note that in this molecular dynamics calculation forces acting on tail atoms were neglected.

(9) Wang, J.; Pullman, A. *Biochim. Biophys. Acta* **1990**, *1024*, 10-18.

(10) (a) Milik, M.; Skolnick, J. *Proc. Natl. Acad. Sci. U.S.A.* **1992**, *89*, 9391-9395. (b) Milik, M.; Skolnick, J. *Proteins: Struct., Funct., Genet.* **1993**, *15*, 10-25.

(11) Deamer, D. W.; Bramhall, J. *Chem. Phys. Lipids* **1986**, *40*, 167-188.

(12) Deamer, D. W.; Nichols, J. W. *J. Membrane Biol.* **1989**, *107*, 91-103.

0002-7863/94/1516-1490$04.50/0

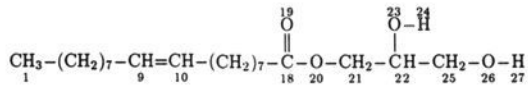

Figure 1. Chemical structure of glycerol 1-monooleate (GMO). The numbering of the atoms corresponds to that used in the text. The head group includes both the carbonyl and glycerol groups (atoms 18–27). The rest of the molecule (atoms 1–17) constitutes the hydrocarbon tail.

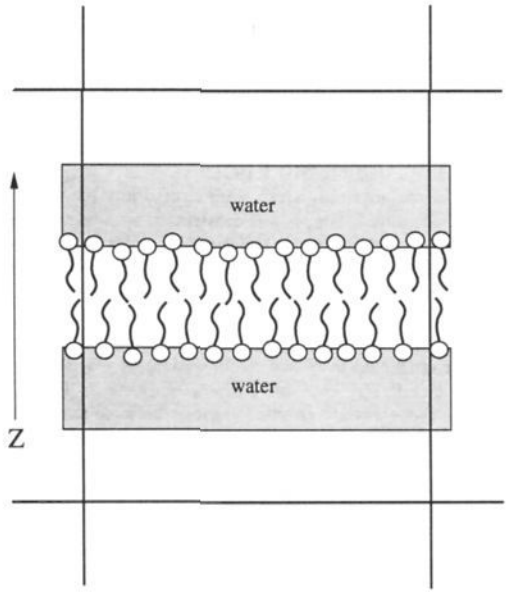

Figure 2. Schematic representation of the water–bilayer system used in the computer simulations. Periodic boundary conditions are applied in all three spatial directions.

at the water–bilayer interface may contribute to the membrane surface potential and influence the efficiency and selectivity of the transport of polar and ionic species across the membrane.[13] It has been further proposed that the surface potential correlates with the exponentially decaying hydration force acting between two membrane surfaces.[14] Testing some of these ideas is the main objective of our work.

II. Methods

Description of the System. A series of MD calculations has been carried out on a system consisting of a GMO bilayer between two water lamellae. The chemical structure of GMO and the numbering of the atoms used in this paper are shown in Figure 1, and a schematic representation of the system is depicted in Figure 2. The bilayer consisted of 72 GMO molecules, arranged with 36 molecules per side. Each water lamella contained 1152 water molecules, corresponding to approximately 8 layers of water. The regions above the upper water lamella and below the lower lamella were low-density water vapor. In addition to the water–bilayer interfaces, the system also contains two water liquid–vapor interfaces. This arrangement was used to ensure that the pressure of the system was low and to allow the thickness of the bilayer to fluctuate as the system equilibrated. The system was placed in a simulation cell of 36.94 Å × 36.94 Å × 150 Å. This yielded a surface area per GMO molecule of 37.9 Å^2, equal to the experimentally determined surface density of a GMO bilayer.[15] The normal to the plane of the bilayer was labeled the z axis. The z dimension of 150 Å ensured that the water molecules in the upper lamella did not interact directly with the periodic images of the water molecules in the lower lamella and vice versa.

Potential Energy Functions. The water–water interactions were described by the TIP4P model,[16] which has been shown to provide a good description of other aqueous interfacial environments, such as the structure of the water liquid–vapor interface,[17] and ions[18] and amphiphilic solutes at this interface.[19,20]

Table 1. Bond Lengths and Bond Angles for GMO

groups	bond length (Å)	groups	bond angle (deg)
C(sp^3)—C(sp^3)	1.530[a]	C(sp^3)—C(sp^3)—C(sp^3)	112.0[a]
C(sp^3)—C(sp^2)	1.500[a]	C(sp^3)—C(sp^2)=C(sp^2)	124.0[a]
C(sp^2)=C(sp^2)	1.380[a]		
C(sp^3)—C(carbonyl)	1.520[b]	C(sp^3)—C(carbonyl)=O	123.0[b]
C(carbonyl)=O	1.200[b]	C(sp^3)—C(carbonyl)—O(ester)	110.0[b]
C(carbonyl)—O(ester)	1.364[b]	O=C(carbonyl)—O(ester)	123.0[b]
O(ester)—C(sp^3)	1.437[b]	C(carbonyl)—O(ester)—C(sp^3)	115.0[b]
C(sp^3)—O(alcohol)	1.430[c]	C(sp^3)—O(alcohol)—H	108.5[c]
O(alcohol)—H	0.945[c]	C(sp^3)–C(sp^3)–O(alcohol)	108.5[c]

[a] See ref 21 for details. [b] See ref 24b for details. [c] See reference 24a for details.

The intermolecular and intramolecular potentials used to describe interactions involving GMO molecules were developed from the OPLS potentials of Jorgensen and co-workers,[21] supplemented with quantum mechanical calculations on ethylene glycol[22] and glycerol.[23] In line with the OPLS methodology, all CH_n groups were treated as united atoms, in which hydrogen atoms bonded to a carbon atom are not considered explicitly and the carbon atom carries the total mass of the group. All other atoms, including hydrogen atoms in the O–H groups, were directly included.

The intramolecular potential energy function contained terms describing Coulomb and van der Waals interactions between atoms separated by at least 3 bonds and rotations around torsional angles:

$$E_{pot} = \sum_i \sum_{<j} \frac{q_i q_j}{R_{ij}} + \sum_i \sum_{<j} 4\epsilon_{ij}\left[\left(\frac{\sigma_{ij}}{R_{ij}}\right)^{12} - \left(\frac{\sigma_{ij}}{R_{ij}}\right)^{6}\right] + \sum_{tors} \frac{V_n}{2}[1 + \cos(n\theta - \theta_{eq})] \quad (1)$$

Here R_{ij} is the distance between atoms (or united atoms) i and j and q_i is the partial charge on atom i. θ, n, and θ_{eq} are the torsional angle, its multiplicity, and its phase. V_n, ϵ_{ij}, and σ_{ij} are empirical parameters depending on atom types. All bond lengths and bond angles were constrained to their equilibrium values which are listed in Table 1.

The potential parameters describing interactions involving hydrocarbon tails of GMO were taken directly from the OPLS parametrization.[21] Since there is no OPLS torsional parameters for the double bond in GMO, a large (but otherwise arbitrary) torsional potential was added to ensure that this bond remained *cis*. The description of the carbonyl–ester part of the head group was also based directly on the OPLS potentials.[24] The OPLS set of potentials does not provide a torsional term for the rotation around the C–C bond in which one of the carbon atoms is attached to a carbonyl oxygen (atoms 17–18). Since the adjacent C–O torsional angle (atoms 18–20) has the same symmetry as this torsional angle, the OPLS potential parameters for the C–O torsion were used.

To determine the potential energy parameters for the glycerol–based head group, a series of *ab initio* calculations were carried out at the 6-31G** level on an isolated ethylene glycol molecule. The ethylene glycol calculations were helpful in assigning torsional parameters to the O–C and C–C bonds in glycerol. With these torsions, a set of atomic partial charges and van der Waals parameters was fit to the energies and dipole moments obtained from *ab initio* calculations on a set of ten conformations of glycerol.[25] The functional form of the fit included the constraint that each of the two CH_2–O–H units and the CH–O–H unit were charge neutral. The resulting partial charges are in close agreement

(13) Flewelling, R. F.; Hubbel, W. L. *Biophys. J.* **1986**, *49*, 541–552.
(14) Simon, S. A.; McIntosh, T. J. *Proc. Natl. Acad. Sci. U.S.A.* **1989**, *86*, 9263–9267.
(15) White, H. S. *Biophys. J.* **1978**, *23*, 337–347.
(16) Jorgensen, W. L.; Chandrasekhar, J.; Madura, J. D.; Impey, R. W.; Klein, M. L. *J. Chem. Phys.* **1983**, *79*, 926–935.
(17) Wilson, M. A.; Pohorille, A.; Pratt, L. R. *J. Phys. Chem.* **1987**, *91*, 4873–4878.
(18) Wilson, M. A.; Pohorille, A. *J. Chem. Phys.* **1991**, *95*, 6005–6013.
(19) Pohorille, A.; Benjamin, I. *J. Chem. Phys.* **1992**, *94*, 5599–5605.
(20) Pohorille, A.; Benjamin, I. *J. Phys. Chem.* **1993**, *97*, 2664–2670.
(21) Jorgensen, W. L.; Madura, J. D.; Swenson, C. J. *J. Am. Chem. Soc.* **1984**, *106*, 6638–6646.
(22) Costa Cabral, B. J.; Albuquerque, L. M. P. C.; Silva Fernandez, F. M. S. *Theor. Chim. Acta* **1991**, *78*, 271–280.
(23) Van Den Enden, L.; Van Alesnoy, C.; Scarsdale, J. N.; Schafer, L. *J. Mol. Struct.* **1983**, *104*, 471–487.
(24) (a) Jorgensen, W. L. *J. Phys. Chem.* **1986**, *90*, 1276–1284. (b) Briggs, J. M.; Nguyen, T. B.; Jorgensen, W. L. *J. Phys. Chem.* **1991**, *95*, 3315–3322. (c) Briggs, J. M.; Matsui, T.; Jorgensen, W. L. *J. Comput. Chem.* **1990**, *11*, 958–971.
(25) Cieplak, P.; Pohorille, A. Quantum mechanical calculations on glycerol, to be submitted for publication.

Table 2. Nonbonded Inter- and Intramolecular Potential Terms for GMO

group name	GMO atom id[a]	charge (e)	intermolecular ε (kcal/mol)	intermolecular σ (Å)	intramolecular ε (kcal/mol)	intramolecular σ (Å)
CH_3	1		0.175	3.905	0.0074	4.0
CH_2	2–8, 11–16		0.118	3.905	0.0074	4.0
CH	9,10		0.115	3.8	0.0074	4.0
CH_2	17	0.05	0.118	3.905	0.0074	4.0
C	18	0.55	0.105	3.75	0.0074	4.0
O	19	–0.45	0.21	2.96	0.17	3.07
O	20	–0.40	0.17	3.00	0.17	2.90
CH_2	21, 25	0.25	0.118	3.905	0.0074	4.0
CH	22	0.25	0.08	3.85	0.0074	4.0
O	23, 26	–0.60	0.17	3.07	0.17	2.90
H	24, 27	0.35				

[a] See Figure 1.

Table 3. Intramolecular Torsional Parameters for GMO[a]

groups	V_1	V_2	V_3
C—C—C—C[b]	1.411	–0.271	3.145
C—C—C—C(sp^2)	1.411	–0.271	3.145
C—C—C(sp^2)=C(sp^2)	0.343	–0.436	–1.121
C—C(sp^2)=C(sp^2)—C	3.000	16.000	0.000
C—C—C(carbonyl)—O(ester)	4.980	6.200	0.000
C—C(carbonyl)—O(ester)—C	4.980	6.200	0.000
C(carbonyl)—O(ester)—C—C	8.918	1.511	2.349
O(ester)—C—C—O(alcohol)	13.753	–3.860	5.147
O(alcohol)—C—C—O(alcohol)	13.753	–3.860	5.147
O(ester)—C—C—C	–2.476	–0.202	–0.335
O(alcohol)—C—C—C	–2.476	–0.202	–0.335
C—C—O(alcohol)—H[c]	2.947	–1.107	1.333
C—C—O(alcohol)—H[d]	1.474	–0.554	0.667

[a] The convention here was to use all heavy atoms to form the torsions. For bonds which form multiple torsions (bonds 17–18, 18–20, 21–22, 22–23, and 22–25 in GMO), boths sets of atoms defining the torsional angle were used. Since the bond lengths and angles are constrained, the division is somewhat arbitrary. [b] Unless otherwise indicated, carbons are sp^3. [c] Terminal alcohol torsion, in GMO bond 25–26. [d] Middle alcohol torsions, in GMO bond 22–23.

with the charges that reproduce the electric field around the ten conformations of glycerol obtained from the recent *ab initio* calculations at the 6-31G** level.[25]

The complete list of partial charges and nonbonded parameters is given in Table 2, and the torsional parameters are listed in Table 3. The GMO–GMO intermolecular potentials between nonbonded atoms of different types and the water–GMO potentials were obtained from the standard OPLS combination rules.[21]

All intermolecular interactions were truncated smoothly by using a cubic spline function.[26] For the water molecules, the oxygen atom was used as the cutoff center. The GMO molecules were subdivided into small charge-neutral groups and the truncation was applied to the distance between the cutoff center of each group. In the head group region of the molecule, these charge-neutral groups consisted of the ester group and two "alcohol" groups. The ester group contained atoms 17–21 with the carbonyl carbon chosen as the cutoff center. The "alcohol" groups contained atoms 22–24 and 25–27 with cutoff centers on oxygen atoms 23 and 26, respectively. The hydrocarbon tail of the GMO molecule, which does not contain atoms carrying partial charges, was divided into six groups of two or three united atoms each. The groups consisted of atoms 1–3 (2), 4–6 (5), 7–8 (7), 9–10 (9), 11–13 (12), and 14–16 (15), where the cutoff atoms are listed in parenthesis. The interactions involving these groups were truncated between 6.5 and 7.0 Å, while the interactions between two groups whose atoms carried partial charges were truncated between 7.5 and 8.0 Å. Note that the cutoffs apply only to the intermolecular interactions; no cutoffs were applied to the intramolecular nonbonded terms.

It should be pointed out that long-ranged effects are not taken into account in this model of intermolecular interactions. These effects are likely to play a significant role in determining the structure and stability of bilayers built of charged monomers. However, they are probably less important when a bilayer consists of uncharged (and non-zwitterionic) molecules, such as GMO. Furthermore, conventional methods for treatment of long-range effects in bulk systems[27] do not appear to be appropriate for interfaces. New approaches have recently been developed specially for interfacial problems,[28] but it is not clear if they are applicable to the present problem.

Molecular Dynamics. The MD trajectories were generated with the Verlet[29] algorithm by the COSMOS program of Owenson and Pohorille.[30] In all cases the temperature was 300 K. SHAKE[31] was applied to constrain all bond lengths and angles. A time step of 0.005 ps was used throughout the simulations, which yielded satisfactory energy conservation. Periodic boundary conditions in the x, y, and z direction were applied in all calculations. The methodology was similar to that used in our work on liquid–vapor systems,[17,32] and more details can be found there.

One of the important concerns in simulating large molecular systems is to ensure that they are thermally equilibrated, so that analyzed trajectories are independent of initial conditions. We addressed this issue by generating five separate MD trajectories. Three trajectories were initiated from configurations which were structurally very different. In the first configuration, a bilayer was constructed with no water present, with the initial conformations of the GMO molecules sampled from the thermal distribution for monomers. The neat bilayer was aged for about 0.1 ns. The water lamellae were then added on both sides of the bilayer. The second configuration was built from a bilayer in which all acyl chains were initially in the *all-trans* conformation. The third starting configuration was constructed from two configurations of a GMO monolayer on a water lamella by combining them tail-to-tail. Thus, in this configuration there was no initial penetration between the two sides of the bilayer. The three initial configurations were subsequently aged for 1.0 ns, each. The remaining two trajectories were started only when the production phases of the second and third run were completed. Then, final configurations of these runs were used to generate new initial structures by periodically randomizing the velocities from the Boltzmann distribution for 50 ps, followed by 50 ps of normal trajectory.

Each of the five trajectories was run for 1 ns after equilibration and analyzed separately. It was found that the results were the same to within their statistical uncertainties. This can be taken as an indication that the systems were well-equilibrated. The analysis presented below contains the results of all five trajectories, for a total length of 5 ns.

III. Results and Discussion

Density Profiles. Probably the most direct measure of the structure of the bilayer–water interface are the atomic density profiles along the interface normal. The profiles of the water molecules, the GMO head groups, and the hydrocarbon tails are shown in Figure 3. As expected, the head groups are localized at the water–bilayer interface while the tails form the hydrophobic core of the membrane. The equimolar surfaces of water, defined as the surfaces where the density on the bilayer side is balanced by the depletion of density on the liquid side,[33] are located at ±16.5 Å. Thus the *total* width of the bilayer, measured as the distance between these surfaces, is about 33 Å, comparable with the value obtained in low-angle X-ray-diffraction experiments on GMO bilayers in the lamellar state. In these experiments, bilayer thicknesses ranged from 33 to 37 Å, depending upon the amount of water present.[34] As our computer simulations were done at a slightly lower surface density (larger surface areas per head group) than the X-ray experiments, a slightly thinner bilayer would be expected. Since GMO is a fairly small bilayer-forming amphiphile, GMO bilayers are thinner than most phospholipid bilayers at 300 K.

(26) Andrea, T. A.; Swope, W. C.; Andersen, H. C. *J. Chem. Phys.* **1983**, *79*, 4576–4584.

(27) See, e.g.: Allen, M. P.; Tildesley, D. J. *Computer Simulation of Liquids*; Oxford University Press: New York, 1987; Chapter 5.5.

(28) (a) Rhee, Y. J.; Halley, J. W.; Hautman, J.; Rahman, A. *Phys. Rev. B* **1989**, *40*, 36–42. (b) Hautman, J.; Halley, J. W.; Rhee, Y. J. *J. Chem. Phys.* **1989**, *91*, 467–472. (c) Hautman, J.; Klein, M. L. *Mol. Phys.* **1992**, *75*, 379–395.

(29) Verlet, L. *Phys. Rev.* **1967**, *159*, 98–103.

(30) Owenson, B.; Pohorille, A. COSMOS—A software package for COmputer Simulation of MOlecular Systems, NASA-Ames Research Center, Moffett Field, CA, 1987.

(31) Cicotti, G.; Ryckaert, J. P. *Comput. Phys. Rep.* **1986**, *4*, 345–392.

(32) Pohorille, A.; Wilson, M. A. *J. Mol. Struct. (Theochem)* **1993**, *284*, 271–298.

(33) Rowlison, J. S.; Widom, B. *Molecular Theory of Capillarity*; Claredon: Oxford, 1982.

(34) Pezron, I.; Pezron, E.; Bergenstahl, B. A.; Claesson, P. M. *J. Phys. Chem.* **1990**, *94*, 8255–8261.

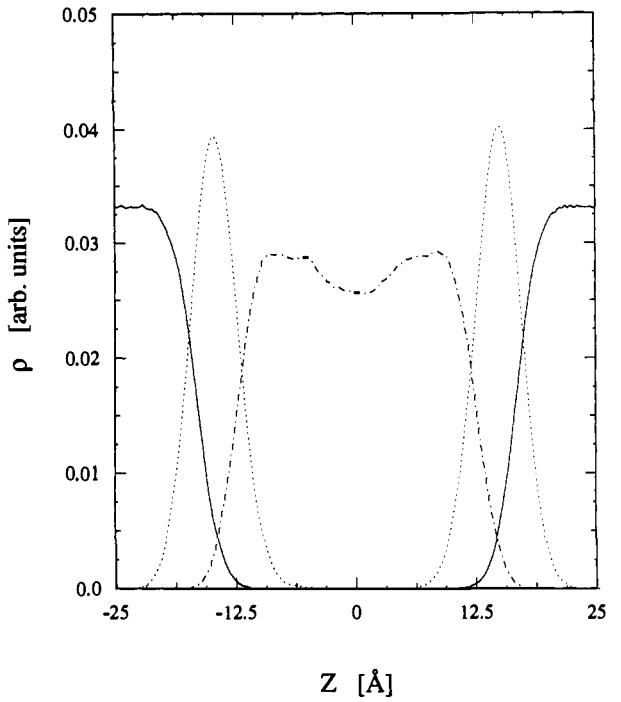

Figure 3. Density profiles of water (solid lines), GMO head group atoms (atoms 18–27) (dotted lines), and alkyl chain united atoms (atoms 1–17) (dash-dotted line) as a function of the coordinate perpendicular to the interfaces.

It is expected that the polar head groups will markedly perturb the interfacial water. This perturbation, however, has no significant influence on the water density profile, which is quite similar to the profile at the water liquid–vapor interface. In particular, as is clear from Figure 3, no density oscillations are present in the interfacial region. The distance over which the water density changes from 90% to 10% of its bulk value (called the 10%–90% width) is approximately 5 Å, compared to 4 Å for the liquid–vapor interface of water. This slight broadening of the density profile at the bilayer interface is probably due to attractive interactions between water molecules and GMO head groups. The observed smoothness of the density profile is in agreement with results of recent simulations[5-7,35] which allowed the water–bilayer interface to fluctuate freely. In contrast, other recent computer simulations of bilayer systems,[36] which either included constraining forces restricting the head groups to a planar surface or were rather short, predicted strong water layering near the membrane. The density oscillations observed in constrained calculations are most likely due to artificial rigidity of the bilayer interface which introduces wall-like correlations in the water density profiles.[37]

The overlap between the density profiles of water and the bilayer components conveys some information on water penetration into the membrane. As we see in Figure 3, the density profile of water significantly overlaps the profile of the head-group atoms (atoms 18–27) which is centered near ±15 Å and has a full width at half maximum (fwhm) of about 5.5 Å. This indicates that water molecules penetrate into the head group region and the polar constituents of the head group are, at least partially, solvated. In contrast, the degree of overlap between the density profiles of water and the tail atoms is significantly smaller. Similar results were obtained in computer simulations of interfaces between water and DLPE bilayer,[5,6] micelles,[38] hexanol,[39] octanol, hexane, dodecane,[40] and dichloroethane,[41] and are consistent with experimental data on water–membrane systems.[42] Water penetration into the hydrocarbon core of a bilayer was observed only in a MD study of interfaces between water and decanoate/decanol membranes.[7] This may be due to the fact that components of this mixed bilayer were distributed nonuniformly, according to their polarity. The head groups of less polar decanol molecules, which were partially buried in the bilayer, could still attract some water molecules and cause broadening of their density profile. In addition, it should be noted that overlap between density profiles does not necessarily indicate molecular-scale penetration between the phases in contact, as some overlap would be expected from capillary wave-type fluctuations of the interface. This issue will be discussed more fully later in the paper.

The width of the hydrocarbon core of the bilayer, defined as the fwhm of the tail groups of the GMO molecules (atoms 1–17), is about 25 Å, in excellent agreement with the results of conductance measurements on GMO bilayers, which estimated the thickness of the hydrocarbon interior to be 25.06 Å at 20 °C.[15] An interesting feature of the density profile is the presence of a considerable minimum in the center of the bilayer. In recent X-ray diffraction studies on phospholipid bilayers, the electron density across the bilayer exhibited similar behavior.[43] This effect was also seen in computer simulation results of DLPE bilayers.[6] The minimum is a result of limited interpenetration of the tails from the two sides of the bilayer. Increasing the interpenetration would restrict the rotational freedom of the tail ends and decrease conformational entropy which would not be offset by energetic gains due to increased van der Waals interactions. In general, the conformational constraints imposed on the tails reduce packing efficiency in the core of the bilayer. The average density of carbon atoms in the core is about 15% lower than the bulk density of 9-octadecene, which has the identical structure of the tail portion of a GMO molecule.

More detailed information about the ordering inside the bilayer can be obtained from the density profiles of individual atoms along the hydrocarbon chains. Several of these profiles are shown in Figure 4. The carbonyl carbon atoms, C(18), are well-localized near the interface with water. The density profile of the carbon atoms which form the double bond, C(9)=C(10), is much less localized, exhibiting two broad, overlapping peaks. The profile of the terminal carbon atoms of the tail, C(1), is even broader. These atoms span the entire bilayer interior, occasionally even moving very close to the surface. In fact, the density profiles of the individual atoms along the hydrocarbon tail become progressively broader toward the end of the tail, indicating increasing disorder in this direction. This is consistent with experimental results which also indicate that the interior of the GMO bilayer is extremely disordered.[15,34,43]

This high degree of disorder is characteristic of bilayers whose hydrocarbon chains are in the fluid state. In contrast, a series of recent neutron and X-ray experiments on phospholipid bilayers in the gel state yielded fairly sharp atomic density profiles.[44] Probably the most important, and often closely related, factors determining the fluidity of hydrocarbon chains are the surface coverage per head group and the presence of unsaturated bonds in the tail region.[45] This can be seen, for example, from the comparison of monolayers of GMO with glycerol–monopalmitin

(35) Wilson, M. A.; Pohorille, A. In *Water–Biomolecule Interactions*; Palma, M. U., Palma-Vitorelli, M. B.; Parak, F., Eds.; SIF: Bologna, 1993; pp 227–230.
(36) (a) Engelmann, A. R.; Medina Llanos, C.; Nyholm, P. G.; Tapia, O.; Pascher, I. *J. Mol. Struct. (Theochem)* **1987**, *151*, 81–102. (b) Nicklas, K.; Böcker, J.; Schlenkrich, M.; Brickmann, J.; Bopp, P. *Biophys. J.* **1991**, *60*, 261–272.
(37) Lee, C. Y.; McCammon, J. A.; Rossky, P. J. *J. Chem. Phys.* **1984**, *80*, 4448–4455.
(38) Shelley, J.; Watanabe, K.; Klein, M. L. *Int. J. Quantum Chem. QBS* **1990**, *17*, 103–117.
(39) Gao, J.; Jorgensen, W. L. *J. Phys. Chem.* **1988**, *92*, 5813–5822.
(40) Wilson, M. A.; Pohorille, A. MD study of the water–hexane, water–dodecane, and water–octanol systems, to be submitted for publication; see also ref 32.
(41) Benjamin, I. *J. Chem. Phys.* **1992**, *97*, 1432–1445.
(42) Casal, H. L. *J. Phys. Chem.* **1989**, *93*, 4328–4330.
(43) Simon, S. A.; McIntosh, T. J.; Magid, A. D.; Needham, D. *Biophys. J.* **1992**, *61*, 786–799.
(44) (a) Wiener, M. C.; King, G. I.; White, S. H. *Biophys. J.* **1991**, *60*, 568–576. (b) Wiener, M. C.; White, S. H. *Biophys. J.* **1991**, *59*, 174–185.
(45) Milik, M.; Kolinski, A.; Skolnick, J. *J. Chem. Phys.* **1990**, *93*, 4440–4446.

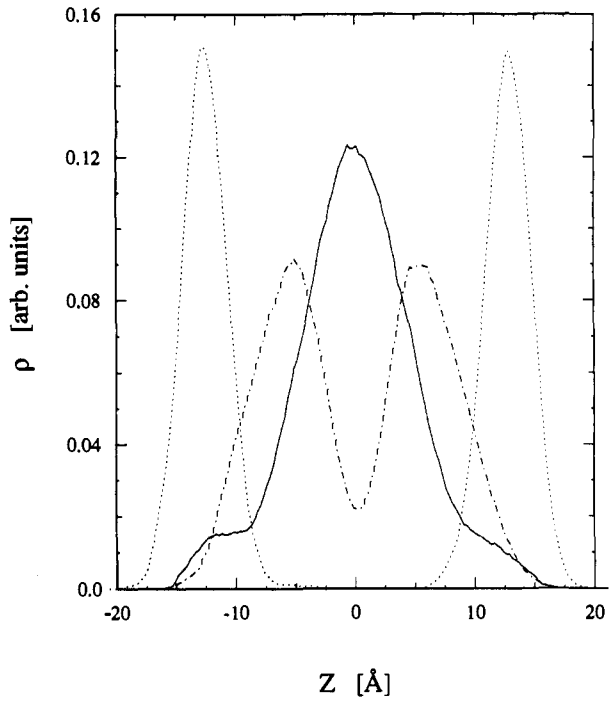

Figure 4. Density profiles of the terminal methyl groups (solid line), the C(9)=C(10) double bond atoms (dash-dotted line), and the C(18) carbonyl carbon atoms (dotted lines) of the GMO alkyl chains as functions of the coordinate perpendicular to the interfaces.

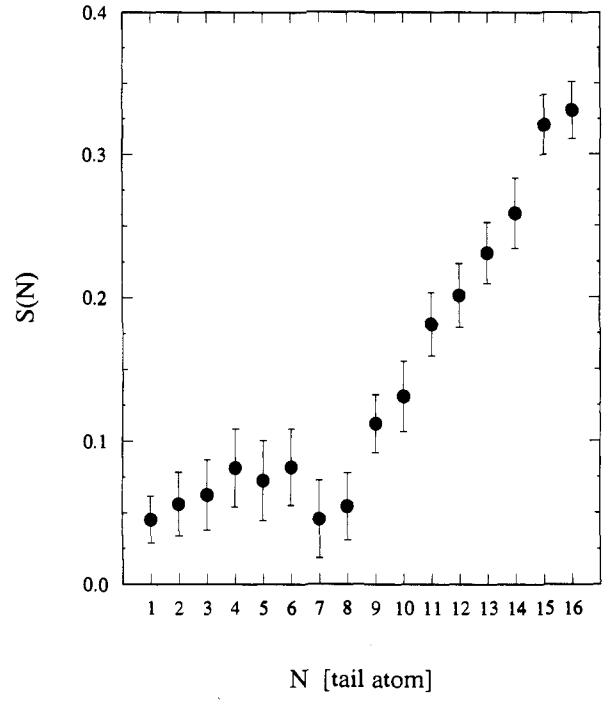

Figure 5. NMR order parameters of next-nearest neighbors, $S_{i,i+2}$, along the alkyl chain of the GMO molecule. The error bars represent ±2 standard deviations.

(GMP) monolayers on water. The main structural difference between these two molecules is the absence of the C(9)=C(10) double bond in GMP. As a result, the surface coverage of the GMP monolayers is only 22.5 Å^2 per molecule[34] and its chain melting temperature is approximately 330 K,[34] over 50 deg higher than that for GMO. Recent computer simulations of GMO and GMP monolayers showed that the chains in the GMO monolayer exhibit a similar degree of disorder as in the bilayer while the GMP monolayer was quite ordered.[35] The monolayer and the present bilayer simulations applied the same potential energy functions, demonstrating that these potentials are successful in describing both fluid and gel states. Thus, it is unlikely that the high degree of disorder found in the GMO bilayer interior is an artifact of inaccuracies in the potential functions.

Structure of the Bilayer. The density profiles of individual atoms, discussed in the previous section, provide information about the distribution of atomic positions inside the bilayer. This information can be complemented by knowledge of the orientational preferences of different chain segments. One quantity that characterizes these preferences is the next-neighbor order parameter, $S_{i,i+2}$, defined as

$$S_{i,i+2} = {}^1/_2(3\langle\cos^2\theta\rangle - 1) \qquad (2)$$

where i and $i+2$ are two carbon atoms along the chain separated by two bonds, θ is the angle between the vector $\mathbf{R}_{i,i+2}$ joining these atoms and the direction normal to the bilayer, and $\langle\ldots\rangle$ represents a statistical average.[46] $S_{i,i+2}$ can assume any value between 1 and −0.5. When $S_{i,i+2} = 1$, $|\mathbf{R}_{i,i+2}|$ is exactly parallel to the normal, when $S_{i,i+2} = -0.5$, $\mathbf{R}_{i,i+2}$ is exactly perpendicular to the normal, and when the distribution of $\mathbf{R}_{i,i+2}$ vectors is random, $S_{i,i+2}$ assumes values near 0. The same order parameter was studied in recent molecular dynamics simulations of the liquid–vapor interfaces of hydrocarbons[47] and DLPE bilayers.[6] $S_{i,i+2}$ is closely related to the conventional NMR order parameter S. To obtain the order parameter as a function of the position in the chain from NMR studies, the hydrogen atoms bonded to successive carbon atoms along the hydrocarbon chain are labeled and θ is defined as the angle between the C–D bond vector and the bilayer normal. In principle, we could obtain S from our simulations even though we have been using a united-atom model without explicit hydrogen atoms. This could have been done by constructing C–H bond vectors with appropriate hybridizations after configurations of the chains were generated in the simulations. This procedure, however, is unnecessary since both $S_{i,i+2}$ and S contain very similar information. In fact, $S_{i,i+2}$ corresponds to the order parameter S_{mol} also used for interpreting NMR data.[46]

The next-neighbor order parameters are plotted in Figure 5 as a function of the first atom in each pair. It is immediately apparent that the vectors near the terminal methyl group (i = 1–6) are much more disordered than the vectors near the head group (i = 9–16) and the position of the double bond (i = 7 and 8) marks a qualitative break between the two types of behavior. A slight dip in the value of the order parameter is observed near this position. A similar dip, found in NMR experiments on phospholipids with oleic acyl chains,[46] has been attributed to the fact that the most probable orientation of the *cis* double bond is slightly tilted away from the bilayer normal. This also appears to be the case for GMO.

Although the NMR order parameters for GMO bilayers have not been measured, the results for phospholipid bilayer indicate that, in general, atoms close to the head group have larger values of order parameters than atoms near the chain end.[46,6] This has also been seen in computer simulations on monolayers[48] and in lattice models of chain assemblies.[45] However, the magnitude of the order parameters observed here is smaller than that in phospholipid bilayers, which again demonstrates that GMO bilayers are highly disordered.

While order parameters provide useful, "collective" information about orientational preferences along the hydrocarbon chain which can be directly compared with experimental results, they do not allow for answering more detailed questions about these preferences. Specifically, is the double bond indeed tilted with respect to the bilayer normal, as indicated above? Is the most probable orientation of the disordered part near the end of the chain perpendicular to the interface or is there a tilt induced by the double bond? These questions can be answered by analyzing the

(46) Seelig, J.; Seelig, A. *Q. Rev. Biophys.* **1980**, *13*, 19–61.

(47) Harris, J. G. *J. Phys. Chem.* **1992**, *96*, 5077–5086.

(48) (a) Karaborni, S.; Toxvaerd, S. *J. Chem. Phys.* **1992**, *96*, 5505–5515. (b) Biswas, A.; Schurmann, B. L. *J. Chem. Phys.* **1991**, *95*, 5377–5386.

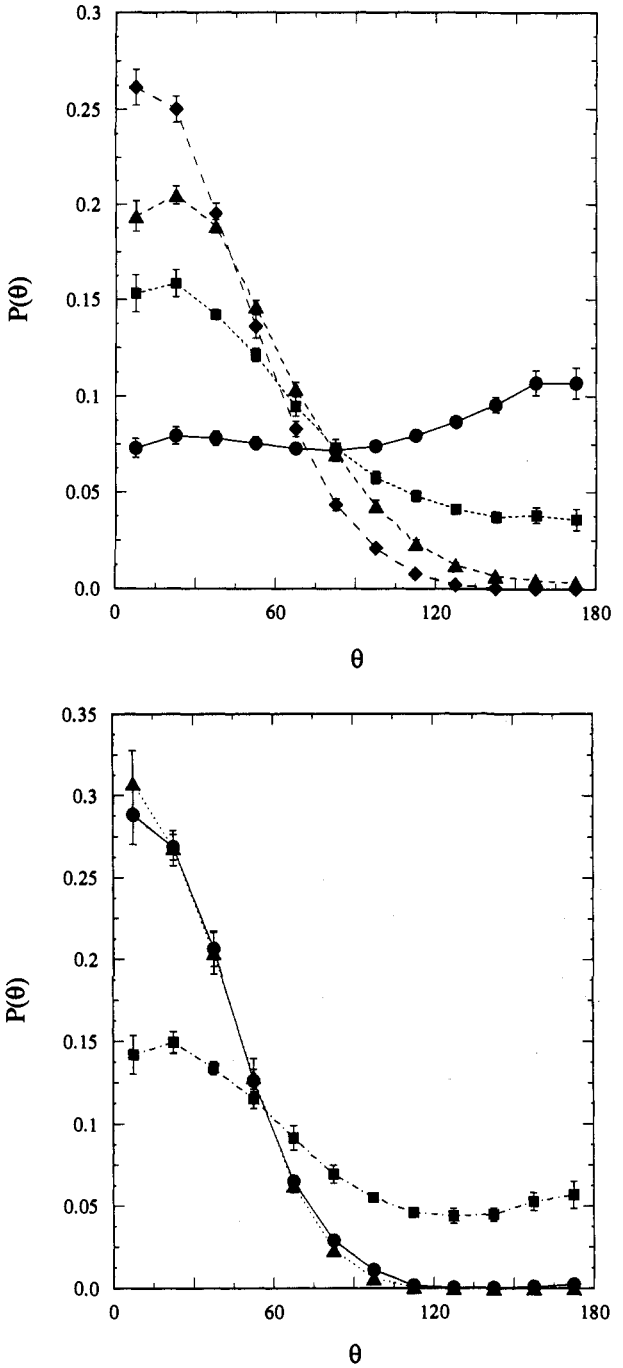

Figure 6. (a, top) Orientational probability distributions of the angle between the bilayer normal (pointing from the bilayer toward water) and next-nearest neighbor vectors in the GMO tail: P_{1-3} (circles), P_{5-7} (squares), P_{9-11} (triangles), and P_{13-15} (diamonds). (b, bottom) Same as in part a, but for vectors from longer tail segments: P_{1-18} (circles), P_{1-9} (squares), and P_{10-18} (triangles).

probability distributions, $P_{i-j}(\theta)$, of observing an angle θ between the vector joining atoms i and j and the bilayer normal (z axis). The distributions are defined as

$$P_{i-j}(\theta) = \langle N(\theta)/\sin(\theta) \rangle \qquad (3)$$

where $N(\theta)$ is the fraction of the total number of vectors which forms an angle $\theta \pm \Delta\theta$ with the bilayer normal, $\sin(\theta)$ corrects for the Jacobian, and $\langle \ldots \rangle$ represents a statistical average. The normal points from the bilayer toward the aqueous phase and the molecular vectors point from atom i to atom j.

The orientational probability distribution functions for several vectors corresponding to the NMR order parameters are shown in Figure 6a. For vectors joining the atoms close to the head group, the distributions are fairly narrow and peak at $\theta = 0$. The

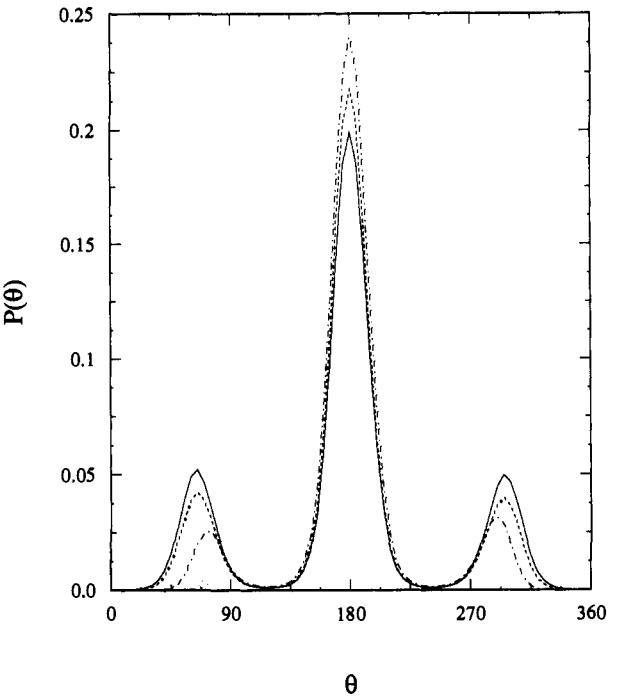

Figure 7. Distributions of torsional angles around C(2)–C(3) (solid), C(12)–C(13) (dashed), and C(16)–C(18) (dot-dashed) in the alkyl tail of GMO.

distributions systematically broaden as the vectors become closer to the methyl end of the chain. The most probable orientation of the $\mathbf{R}_{9-11}$ vector, near the double bond, is shifted away from the normal by about 30°, but it is otherwise similar to the other distributions. The distribution of the $\mathbf{R}_{1-3}$ vector at the free end of the hydrocarbon chain is extremely broad with the maximum near $\theta = 180$. This behavior is due to the connectivity constraints in the terminal methyl group. If the free end of a tail lies near the aqueous–bilayer interface, it is most likely to adopt a "hooked" conformation in which the $\mathbf{R}_{1-3}$ vector points toward the bilayer interior.

The distribution of the tail segment above the double bond, P_{10-18}, shown in Figure 6b, is very strongly peaked near $\theta = 0$, due to the constraints imposed upon the GMO molecules by the water–bilayer interface. In contrast, the distribution of the tail segment below the double bond, P_{1-9}, is fairly broad, but still exhibits a peak near $\theta = 0$. Thus, there is no systematic tilt at the end of the chain induced by the double bond.

The positional and orientational disorder inside the bilayer is, of course, directly related to the conformational flexibility of the hydrocarbon chains. Chain segments can change direction only as a result of transitions between *trans* and *gauche* states. The distributions of several torsional angles along the chain are shown in Figure 7. For the first torsional angle, C(1)–C(2)–C(3)–C(4), a sizable population (about 34%) of the *gauche* states was found. This is similar to the torsional distribution in bulk liquid hydrocarbons.[39] For torsional angles closer to the head groups, there is a clear shift toward the *trans* state, although the *gauche* states still retain a population of about 20%. This behavior again indicates that the interior of the bilayer is quite fluid.

Further evidence for the conformational flexibility of the tails is obtained by analyzing the frequency of transitions between the *trans* and the two *gauche* states. Over the course of the simulation, many such transitions were observed for all the torsions in the tail (with the exception of the torsion around the double bond which remained in the *cis* state). For the first torsional angle the average rate was 0.0186 *trans-gauche* transitions/molecule per ps. For the angle around the bond formed by atoms 16 and 17

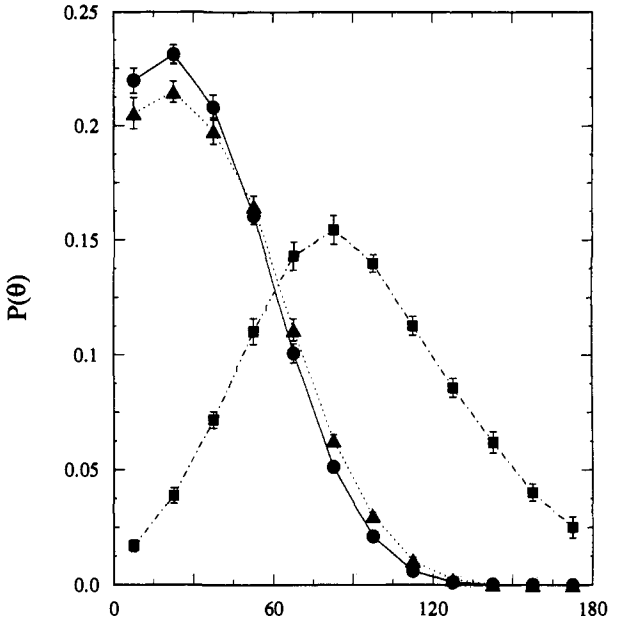

Figure 8. Orientational probability distributions of the angle between the bilayer normal (pointing from the bilayer into water) and head group vectors of P_{18-26} (circles), P_{18-19} (squares), and P_{18-20} (triangles).

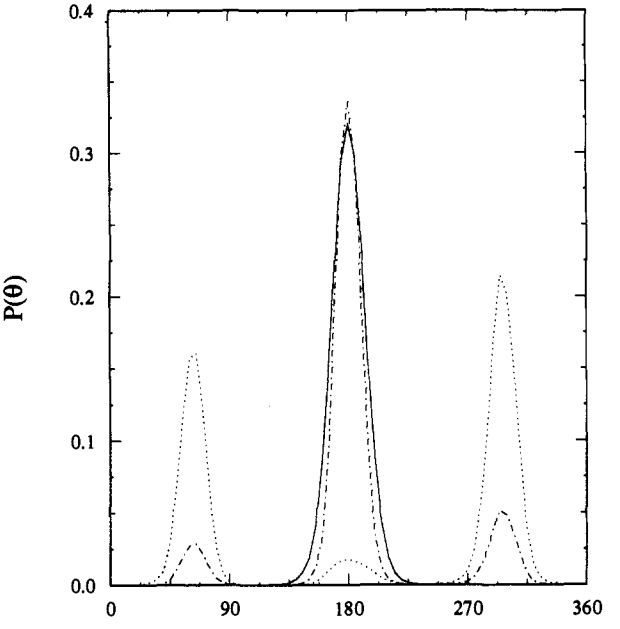

Figure 9. Distributions of torsional angles around bonds O(20)–CH_2-(21) (solid), CH_2(21)–CH(22) (dotted), and CH(22)–CH_2(25) (dot-dashed) in the head group of GMO. The torsion around CH_2(21)–CH(22) is measured along the glycerol backbone (atoms 20–21–22–25), as is the torsion around CH(22)–CH_2(25) (21–22–25–26).

this rate was 0.0106 transitions/molecule per ps. This corresponds to the total of about 6700 and 3800 transitions for all chains over the full length of the trajectories. The smaller number of transitions in torsional angles near the head group, compared with the transitions near the terminal methyl group, is due to the fact that the constraints imposed by orientations of the head groups and by the length of the hydrocarbon tail tend to hamper the torsional freedom around these bonds. The number of transitions occurring during the simulations also supports the argument that the chains have had adequate time to sample their conformational space, so that the resulting statistical averages represent an equilibrium state of the bilayer interior.

A similar orientational and conformation analysis has been carried out on the atoms forming the glycerol ester head group of GMO. The orientational preferences of polar groups in the head group region are likely to play an important role in determining how small molecules interact with the bilayer–water interface. Also, the knowledge about these preferences is needed to establish a connection between macroscopic measurements of surface potential across the bilayer–water and monolayer–water interfaces and the microscopic structure of these interfaces.[49]

The orientational distribution of the vector, P_{18-26}, which connects heavy atoms on both ends of the head group is shown in Figure 8. We see that for the most probable orientation the head group vector is tilted about 25° with respect to the bilayer normal. The distribution, however, is quite broad, so that there is a perceptible probability of finding the head group almost parallel to the surface (note that the distributions are corrected for the Jacobian). Similar distributions were calculated for the C(18)=O(19) and C(18)—O(20) bond vectors involving the carbonyl carbon atom and are also shown in Figure 8. The most probable orientation is such that the C=O vector lies almost parallel to the interface and the C—O vector forms a 30° angle with the surface normal. Again, both distributions are quite broad, indicating significant orientational disorder in the head group region. One consequence of this result is that simple models for molecular-level interpretation of surface potential measurements, which assume rigid orientations of head groups,[49] are not justified.

While the head groups appear to be orientationally flexible, their conformation is fairly rigid. The torsional distributions around O(20)–C(21), C(21)–C(22), and C(22)–CH(25) are shown in Figure 9. These bonds form the main part of the head group backbone. The O(20)–C(21) torsional angle is localized in the *trans* state. The same conformational preference was found in recent computer simulations of liquid methyl acetate,[24b] which contains a very similar torsional angle. Most of conformational flexibility of the head group backbone is in the two glycerol C–C bonds. Quantum mechanical calculations demonstrate that the most stable conformations of an isolated glycerol molecule are stabilized by intramolecular hydrogen bonding between the hydroxyl groups. Similar hydrogen bonds are also formed in the bilayer, despite competition from the O–H groups in the neighboring head groups and from water molecules which penetrate the head group region. As we see in Figure 9, the most probable conformations around the C(21)–C(22) and C(22)–C(25) bonds are *gauche* and *trans*, respectively. This allows for the formation of a hydrogen bond between H(24) and O(26) providing that the C(21)–C(22)–O(23)–H(24) torsional angle is *gauche*$^-$ or *trans*. Indeed, we find that *gauche*$^-$ is the most probable state, while *gauche* is least populated. Similarly, the torsional distribution around C(25)–O(26) shows a slight preference for the *gauche*$^-$ state, the only arrangement in which the terminal O–H group can participate in intramolecular hydrogen bonding.

Structure of Water at the Bilayer Interface. Since the GMO head groups are polar and contain atoms which can form hydrogen bonds, the structure of water in the interfacial region is likely to be quite different from the structure at the liquid–vapor interface. We have already observed that the width of the water density profile at the bilayer interface increases somewhat due to the solvation of the head groups by the water molecules. This effect has also been found in computer simulations of GMO monolayers at different densities at the water liquid–vapor interface.[35]

In our previous work on the water liquid–vapor interface, we analyzed the structure of the interfacial water by examining the net excess z component of the dipole moment in the interfacial

(49) (a) Vogel, V.; Mobius, D. *Thin Solid Films* **1988**, *159*, 73–81. (b) Vogel, V.; Mobius, D. *J. Colloid Interface Sci.* **1988**, *126*, 408–420. (c) Taylor, D. M.; de Oliveira, O. N.; Morgan, H. *J. Colloid Interface Sci.* **1990**, *139*, 508–518; see also discussion in Section 9 of ref 32.

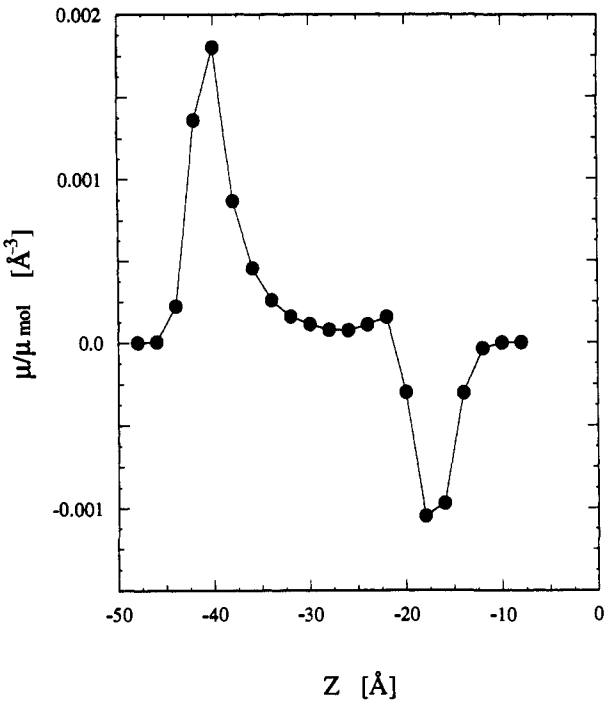

Figure 10. Net z component of the molecular dipole moment density of the water, normalized by the dipole moment of a water molecule. The GMO bilayer is to the right of the water, with the center of the bilayer defining the origin of the coordinate system. The water–bilayer interface is located near −16.5 Å, and the water liquid–vapor interface is located near −37 Å.

region and the orientational distribution functions of the water molecular dipole and the OH bond vectors. The same quantities have been calculated in this work. The results for the excess dipole moment are shown in Figure 10. The orientational distributions of the dipole moments and of the OH bond vectors are displayed in Figure 11.

Water molecules within about 10 Å of the GMO surface are perceptibly polarized by the interface. The net dipole moment at the water–bilayer interface points toward the aqueous phase. Similarly, the net dipole moment at the liquid–vapor interface points from the vapor to the liquid. Thus the overall direction of the water dipoles is preserved from the water–liquid to the water–bilayer interface. The influence of the bilayer surface can be noticed in two features of Figure 10. First, the magnitude of the dipole moment is smaller than that of the water liquid–vapor interface. Second, the direction of the water dipoles is reversed near the bilayer surface. The arrangement of water molecules which penetrate the bilayer and those in the aqueous phase is such that their dipolar interactions with the head groups are energetically favorable. A similar non-monotonic behavior of the water polarization has been observed in computer simulations on DLPE bilayers.[5] For this reason, it has been argued that the water polarization profile is not a suitable order parameter in the Marcelja-Radic theory of hydration forces.[5]

The orientational distributions of the water dipoles in the bilayer reach a maximum near $\theta = 90°$. This preference persists through the equimolar surface to about 4 Å into the water lamella, where the distribution becomes almost uniform. A slight asymmetry of the dipolar distributions is responsible for the excess net dipole moment along the bilayer normal. This is similar to the distribution of the dipoles at the water liquid–vapor interface.[17,50]

Even though the distributions of water dipoles at the water–bilayer and water liquid–vapor interfaces are quite similar, the orientations of the interfacial water molecules are different. This can be seen from the distribution of the OH bond vectors. At

(50) (a) Matsumoto, M.; Kataoka, Y. *J. Chem. Phys.* **1988**, *88*, 3233–3245. (b) Motakabbir, K. A.; Berkowitz, M. L. *Chem. Phys. Lett.* **1991**, *176*, 61–66.

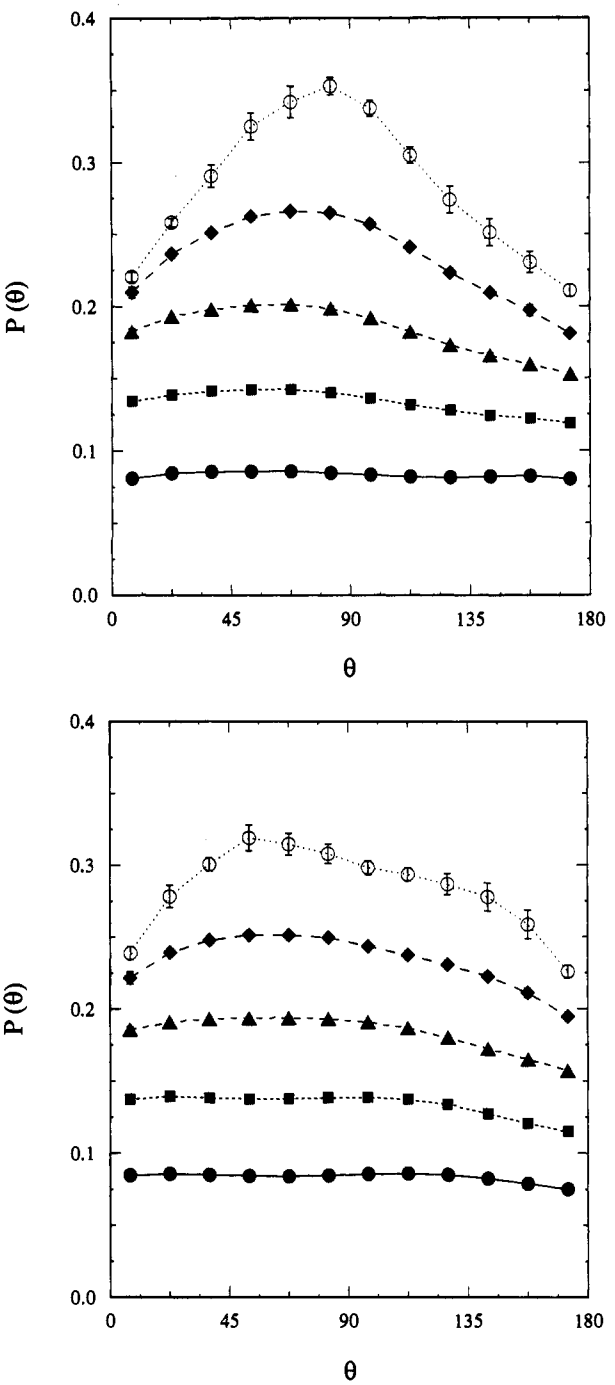

Figure 11. (a, top) Orientational probability distribution of the angles formed by the bilayer surface normal (pointing from the bilayer into water) with the molecular dipole vectors of water molecules between 11 and 13 Å (open circles), 13 and 15 Å (diamonds), 15 and 17 Å (triangles), 17 and 19 Å (squares), and 19 and 21 Å (filled circles); (b, bottom) as in part a, but for the water O–H bond vectors.

the liquid–vapor interface, this distribution is bimodal,[17] with one O–H bond pointing toward the vapor and the other O–H bond directed into the liquid. At the water–bilayer interface, the bimodal distribution is replaced by a very broad distribution, slightly skewed toward low values of θ, which peaks near $\theta = 50°$. Thus, there is a greater probability that the OH vectors point toward the bilayer ($\theta < 90°$) than toward the water lamella.

The density profiles and the distributions of the water dipoles suggest that there is a significant degree of water penetration into the head group region. Probably the most direct way to address this issue is by calculating the pair correlation functions between the oxygen atoms of the head group and the water oxygen atoms. The results are shown in Figure 12. The pair correlation functions involving the hydroxyl oxygen atoms of GMO exhibit

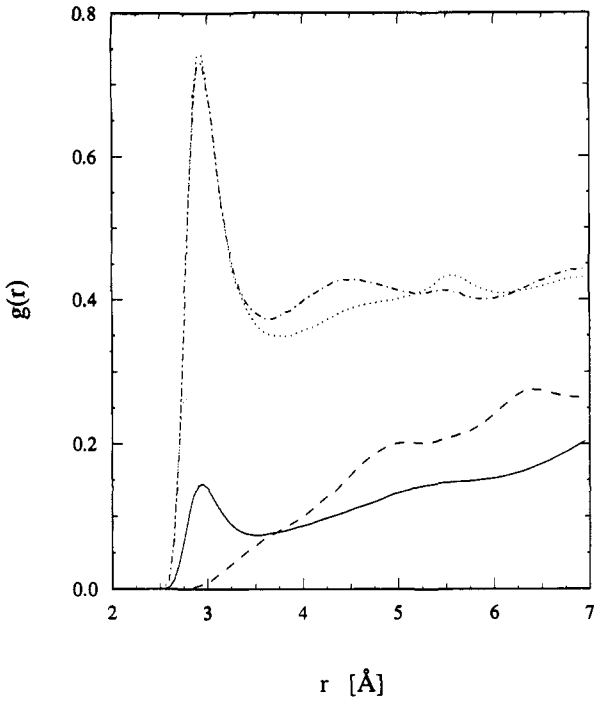

Figure 12. Oxygen (GMO)–oxygen (water) radial distribution functions, $g_{OO}(r)$, for GMO atoms O(19) (solid), O(20) (dashed), O(23) (dotted), and O(26) (dot-dashed) normalized to bulk water.

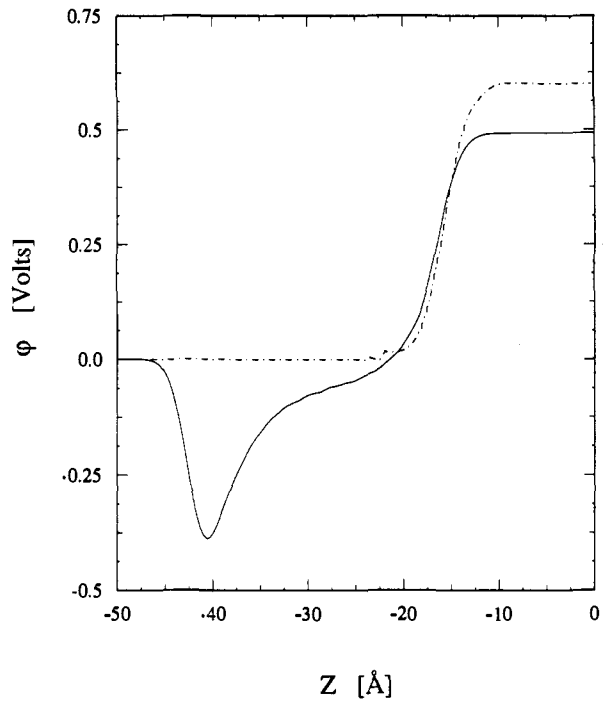

Figure 13. Electrostatic potential across the water–bilayer interface. The contributions from water (solid line) and GMO molecules (dot-dashed line) are shown separately. The center of the bilayer is located at the origin. The water curve exhibits the surface potential across the liquid–vapor interface located at about −37 Å in addition to the water–bilayer interface at −16.5 Å. The net surface potential is the difference in electrostatic potential at the center of the bilayer (origin) and the center of the water lamella (−25 Å).

a pronounced peak at 2.95 Å. This demonstrates that water molecules solvate this part of the head groups. However, it appears that water penetration further into the head group region decreases markedly, such that neither the carbonyl nor the ester oxygen atoms are hydrated to any significant extent.

The surface potential is a measurable macroscopic property which is a sensitive function of the microscopic structure of the interface. It is defined as the drop in electrostatic potential experienced by a test charge crossing the interface. Measurements of the surface potential are commonly used to interpret the molecular structure of monolayers spread on water.[51] The surface potential is also important in theories of transport of ionic species across bilayers. The generally much larger permeability of bilayers to anions than to cations is usually taken as supporting a picture in which the bilayer interface has a net positive surface potential. Furthermore, recent calculations showed that potential difference between the head group region and the core of GMO influences transport of ions through gramicidin channels.[9]

The surface potential, $\Delta\Phi$ across the bilayer-water interface can be obtained by integrating the calculated electric field, $E_z(z)$, in the z-direction

$$\Delta\Phi = \int_{z_1}^{z_2} E_z(z)\,dz \qquad (4)$$

where z_1 and z_2 are located in the middle of the water and bilayer lamellae. The electric field $E_z(z)$ can be expressed as[17,52]

$$E_z(z) = \frac{2\pi\langle q_-(z) - q_+(z)\rangle}{S} \qquad (5)$$

where $q_+(z)$ and $q_-(z)$ are total charges above and below the plane located at height z, S is the xy cross-sectional area of the simulation box and $\langle\ldots\rangle$ represents statistical average.

Unlike $\Delta\Phi$ at the water liquid–vapor interface, the surface potential across the water–bilayer interface, shown in Figure 13, is monotonic and positive in the direction from the aqueous phase into the bilayer. The calculated sign of $\Delta\Phi$ agrees with experiment,[53] but its value of 1.16 Volts is larger than that measured for GMO monolayers on water by a factor of 3–4. The source of this large discrepancy is not clear at this time. The most likely reason is the lack of intramolecular polarization terms in the energy function. Qualitatively, addition of these terms should lower $\Delta\Phi$. Another possible source of error is the neglect of long-ranged forces. Also, if the overall structure of the GMO headgroup was too rigid it would yield an overestimated net dipole moment. We are currently investigating this problem by developing accurate, polarizable model potential functions for describing intra- and intermolecular interactions for glycerol and water-glycerol interactions.

Even though $\Delta\Phi$ is substantially overestimated, it is still possible to gain useful qualitative insight into its origin. The observed surface potential is made up of a contribution of 0.57 V from the water and 0.59 V from the bilayer. Thus the bilayer surface has a strong polarizing influence on the aqueous surface. This supports the picture that the surface potential of the bilayer interface contains important contributions from both the amphiphilic species and the water.[54]

Membrane Thinning and Defects. In this section, we investigate the thermal fluctuations of the membrane surfaces and the nature of the instantaneous defects in these surfaces. This issue has important implications for the transport of material across the bilayer. The measured permeabilities of membranes to water is markedly larger than that expected from solubility-diffusion models assuming a constant average width of the bilayer.[11,12] Similarly, simple ions permeate membranes much faster than predicted from the Born model applied to a fixed membrane width geometry.[12,55] One possible resolution to this disagreement is that fluctuations in the bilayer give rise to deep transient defects and even pores, through which much of the transport occurs.

As we have already pointed out, the time-averaged density profiles do not provide any direct measure of membrane

(51) Mohwald, H. *Annu. Rev. Phys. Chem.* **1990**, *41*, 441–476.
(52) Wilson, M. A.; Pohorille, A.; Pratt, L. R. *J. Chem. Phys.* **1988**, *88*, 3281–3285.
(53) Smaby, J. M.; Brockman, H. L. *Biophys. J.* **1990**, *58*, 195–204.
(54) Gawrisch, K.; Ruston, D.; Zimmerberg, J.; Parsegian, V. A.; Rand, R. P.; Fuller, N. *Biophys. J.* **1992**, *61*, 1213–1223.
(55) For calculations of the Born barrier to ion transport through membranes of fixed widths see: Parsegian, A. *Nature* **1969**, *221*, 844–846.

fluctuations. From Figure 3 it is not possible to distinguish whether the overlap between the water and bilayer profiles is due to the molecular-scale interpretation between these components of the system or to longer wavelength surface fluctuations. To shed light on this problem a microscopic definition of the instantaneous surface is needed. There is, however, no unique way to define such a surface, and several alternatives have been suggested.[56,57] One possibility has been proposed by Weeks,[56] in which the system is subdivided into columns whose size is determined by the bulk correlation length. The equimolar surface of each column is then used to define the microscopic surface, $z(x,y)$. Another definition, proposed by Stillinger, is based on connectivity conditions of the free volumes in the coexisting phases.[57] While these definitions allowed for developing elegant theories for the density distributions and long-range fluctuations at the liquid–vapor interface of single-component substances, their applicability to surfaces formed by large, chemically complex molecules is not clear. Another alternative is to define $z(x,y)$ as a Connolly surface.[58] For this purpose every atom in a given lamella is assigned the van der Waals radius. Then, the surface is defined by rolling a sphere of radius r_C along the excluded volume formed by van der Waals spheres of the surface atoms. This definition, which can be applied to surfaces of any chemical complexity, is particularly suitable for analyzing molecular-scale membrane defects.

Even with these definitions, there is still some degree of arbitrariness in defining an instantaneous surface. The Connolly surface depends upon the size of the probe, r_C, while the Weeks surface depends upon the cross-sectional area of the columns. Therefore, we examined Connolly surfaces determined by probes of radii 1.35 and 1.9 Å, which approximately correspond to the sizes of water and methane molecules, respectively. This not only tests the consistency of the results but also allows identification of defects which could accommodate water molecules and small hydrophobic solutes. The surfaces were constructed for 20 000 configurations equally spaced along the MD trajectories. For each configuration the surface $z(x,y)$ was defined on an x,y-grid of 32 × 32 points.

For a water–bilayer system, there are several microscopic surfaces which can be constructed. The GMO molecules in the bilayer can be used to define upper and lower bilayer surfaces, $z_b^l(x,y)$ and $z_b^u(x,y)$. These individual surfaces can be combined to provide information on thickness fluctuations of the bilayer, $w_b(x,y) = z_b^u(x,y) - z_b^l(x,y)$. Alternatively, the water lamella can be used to define two surfaces adjacent to the bilayer. Conclusions regarding fluctuations of the water–bilayer interface are the same in both cases. Therefore we limit further discussion to $z_b^l(x,y)$ and $z_b^u(x,y)$.

The nature of the fluctuations can be probed by expanding the instantaneous surface functions, $z(x,y)$, in a two-dimensional Fourier series in x and y. The resulting power spectrum of the amplitudes, $A(k)$, is of special interest because there are several theoretical predictions of its functional dependence on the wave vector, k,

$$\langle A(k) \rangle \propto 1/k^n \qquad (6)$$

For example, the capillary wave theory predicts $n = 2$,[33] while pure elastic bending would result in $n = 4$.[59,60] The slope of a log–log plot of the square amplitudes versus k vector is equal to $-n$. Such a plot for the Connolly surfaces obtained by using a probe of radius 1.35 Å is shown in Figure 14. Using a probe of radius 1.9 Å yields a very similar plot. These results are consistent with capillary wave type fluctuations of the surfaces. At low k vectors, the plot is nearly linear with a slope of –2, indicating that

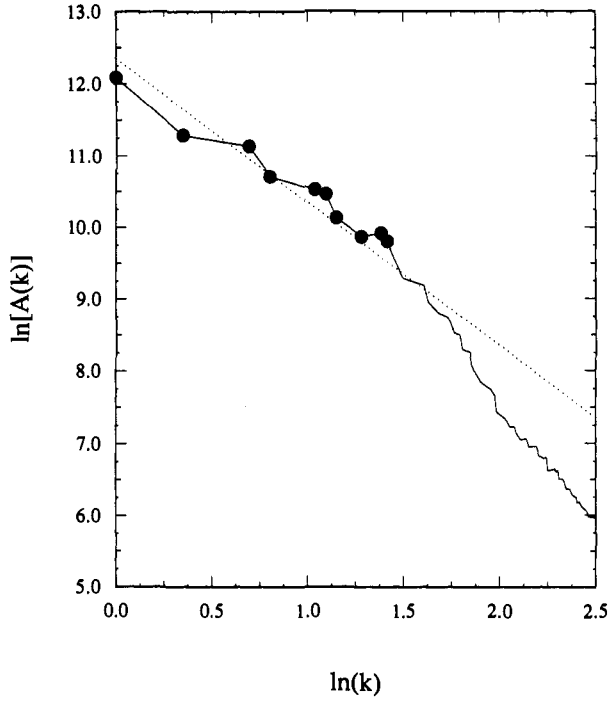

Figure 14. Log–log plot of the power spectrum of fluctuation of the bilayer surface as a function of the k vector. The circles at small ln(k) are included to show the low density of data in this region. The dotted line has a slope of –2.

the fluctuation spectrum varies as $1/k^2$. The linearity of the plot persists to k vectors which correspond to wavelengths of about 7 Å. Then the curve falls off sharply. This is an expected result due to the molecular structure of the interface at these shorter wavelengths. The spatial resolution of 7 Å corresponds roughly to the bulk correlation length for water and the width of the glycerol head group. This behavior is seen for all the surfaces we have considered, including the individual water and bilayer surfaces, as well the bilayer width.

Additional information about surface fluctuations has been obtained by binning the calculated values of $z_b^l(x,y)$ and $z_b^u(x,y)$ for each x,y gridpoint and each instantaneous surface. This yields the probability distribution, $P_b(z)$, of the location of the instantaneous bilayer surface. For a surface undergoing capillary wave fluctuations, $P_b(z)$ is expected to be Gaussian. The same procedure applied to $w_b(x,y)$ yields the probability distribution, $P_b(w)$, of the instantaneous width of the bilayer. These probability distributions for the individual upper and lower bilayer surfaces and for the width of the bilayer are shown in Figure 15. For the Connolly upper and lower bilayer surfaces, the peaks of $P_b(z)$ are at $z = 18.1$ Å and $z = -17.8$ Å, respectively, and $P_b(w)$ has the maximum at $z = 36.7$ Å. As shown in Figure 15, all distributions are Gaussian to within the statistical uncertainties of our calculations. The calculated variances of $P_b(z)$ and $P_b(w)$ are 4.3 and 8.3 Å^2, respectively. Thus, the width of the Gaussian associated with the thickness fluctuations is about twice that of the individual surface distributions, which implies that the upper and lower bilayer surfaces fluctuate independently. While the actual widths of the distributions depend upon the particular definition of the surface, the observations regarding the Gaussian nature of the distributions and the relationship between $P_b(z)$ for the individual surfaces and the thickness of the bilayer do not. This holds true not only for the Connolly surfaces, but also for the distributions calculated for the Weeks surfaces.

The small-width tail of $P_b(w)$ is worth careful examination since it measures the probability of observing deep transient thinning defects in the bilayer. Such defects were previously noticed in lattice model simulations of bilayers.[61] Here, using

(56) Weeks, J. D. *J. Chem. Phys.* **1977**, *67*, 3106–3121.
(57) Stillinger, F. H. *J. Chem. Phys.* **1982**, *76*, 1087–1091.
(58) Connolly, M. L. *Science* **1983**, *221*, 709.
(59) Landau, L. D.; Lifshitz, E. M. *Theory of Elasticity*; Pergamon: Oxford, 1970; Chapter II.
(60) Helfrich, W. *Z. Naturforsch.* **1978**, *33a*, 305–315.
(61) Owenson, B.; Pratt, L. R. *J. Phys. Chem.* **1984**, *88*, 2905–2915.

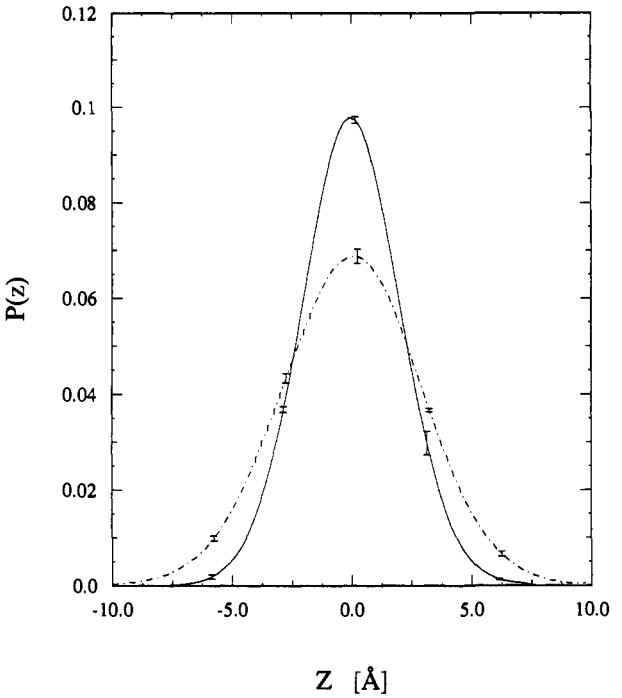

Figure 15. Probability distribution of the fluctuations of the instantaneous bilayer surfaces, $P_b(z)$ (solid line), and the instantaneous width of the bilayer, $P_b(w)$ (dot-dashed line). For better comparison, maxima of both distributions were shifted to $z = 0$. $P_b(z)$ is averaged over the lower and upper surfaces.

the Connolly surfaces defined by the probe of the size of a water molecule, we occasionally find defects as deep as 15 Å. This corresponds to a local width of the bilayer of only 20 Å. When the probe has the size of a methane molecule, defects of the order of 10 Å are found. It is worth noting that $P_b(w)$ is described by a Gaussian function in the whole small-width range. This is not an obvious result since one could speculate that the formation of deep, molecular-scale defects might result from a different molecular mechanism than the mechanism leading to capillary fluctuations around the average width.

The analysis of bilayer fluctuations, presented above, does not explicitly address the molecular mechanism through which they occur. Two possibilities can be envisioned. In the first possible mechanism, fluctuations are produced by the motion along the interfacial normal of the whole GMO molecules. In the second possible mechanism, fluctuations result from conformational and orientational dynamics of the part of GMO molecules close to the surface, mostly head groups. In contrast to the previous case, the tails of the GMO molecules forming the hydrocarbon core would not be markedly affected by fluctuations of the surface atoms.

One way to distinguish between the two mechanisms outlined above is to investigate the density profile of the terminal methyl group of the GMO tail as a function of the head group position perpendicular to the interface. A shift in this density profile from the center of the bilayer for GMO molecules whose head groups exhibit increased exposure to water would be considered as an argument for the first mechanism of surface fluctuations. From Figure 16a it is however clear that the profiles are virtually independent of the degree of penetration of the head groups into the aqueous phase. On the other hand, the orientational distribution of the head groups, $P_{18-26}(\theta)$, shown in Figure 16b, and the length of the head groups, $\mathbf{R}_{18-26}$ (not shown), do depend on the positions of the head groups along the interface normal. As the head groups penetrate into the aqueous phase they adopt, on average, more extended conformations and become better aligned with the bilayer normal, an effect also observed for a single amphiphilic molecule on the water surface.[20] These results

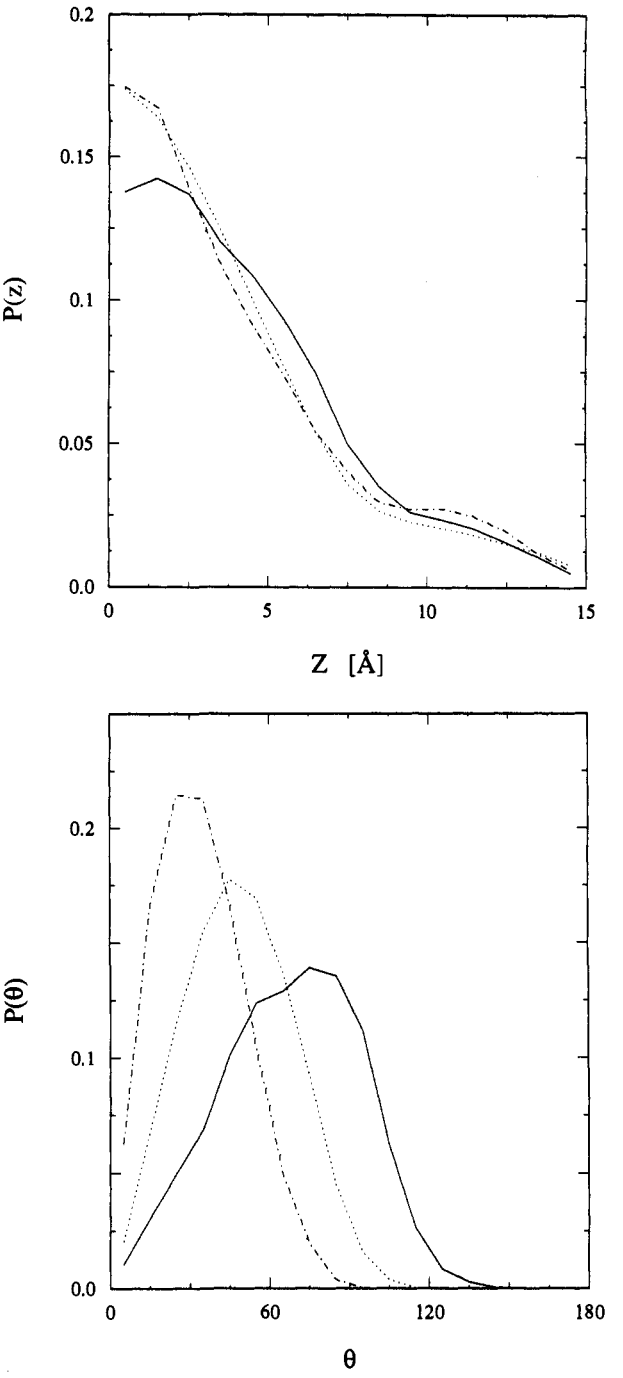

Figure 16. (a, top) Density profile of the terminal methyl group (CH_3-(1)) when the location of the terminal oxygen atom of GMO relative to the center of the bilayer, $z_{O(26)}$, is <14 Å from the center of the bilayer (solid line), 14 Å < $z_{O(26)}$ < 18 Å (dotted line), and 18 Å < $z_{O(26)}$ (dot-dashed line). (b, bottom) Orientational probability distribution of the head group vector pointing from C(18) to O(26) as a function of distance from the COM of the bilayer for different head group locations as defined for part a.

indicate that the dynamics of the head groups is mainly responsible for molecular-level surface fluctuations.

We can further pursue the analysis of molecular-scale fluctuations by asking what types of atoms form the walls of the defects. As it turns out, the "lining" of the defects is strongly hydrophilic. About 70% of atoms within 3.5 Å of the surface probe are oxygen atoms. This number does not depend on the depth of a defect; only the frequency of finding the carbonyl oxygen atoms in deep defects increases at the expense of the hydroxyl oxygen atoms. The remaining 30% are carbon atoms of the head groups; no tail atoms were found near defects.

It should be noted that thinning defects analyzed here are defined in terms of the width of the bilayer only. A number of more complicated cases can be envisioned, such as when a defect in the upper bilayer surface is not directly above a defect in the lower surface. Similarly, worm-like defects which change direction across the bilayer have not been included in our analysis. Thus, the number and size of the observed surface defects should be taken as a lower bound.

IV. Conclusions

In this paper we have presented results of computer simulations of a GMO bilayer in water. The main issues which have been discussed are the structure of a fluid membrane, the structural and electrical properties of the water–bilayer interface, and the nature of membrane fluctuations.

The observed bilayer thickness and structure are in very good agreement with experimental data. Analyses of the NMR order parameters, atomic density profiles, and torsional distributions indicate that the interior of the GMO bilayer is quite fluid and the disorder increases toward the middle of the bilayer. The atomic density is reduced in the center of the bilayer, yielding a density profile that is more complex than assumed by simple models of membranes which treat the bilayer interior as a uniform hydrocarbon phase. Consequently, the solubility of water and nonpolar species in the bilayer may differ markedly from predictions of these models.

The flexibility of the bilayer is not limited to its interior, as the surface also exhibits out-of-plane thermal fluctuations. Such fluctuations, which occur on the time scale of present calculations, were analyzed by performing 2-d Fourier transforms of the instantaneous bilayer surfaces. The resulting power spectrum is in agreement with the capillary wave model of interfacial fluctuations. This is consistent with a Gaussian distribution of the instantaneous width of the bilayer which is twice as broad as the individual bilayer surfaces, indicating that motions of the surfaces are uncorrelated. At present, these conclusions should be considered as limited to very fluid membranes and their extension to more rigid phospholipid bilayers remains to be established. Also, our calculations do not provide information about surface fluctuations which occur on longer time scales and/or larger spatial dimensions. Such fluctuations may include, for example, components from elastic bending.

Fluctuations in the width of the bilayer result in the formation of transient thinning defects. These are created mainly by conformational and orientational changes in the head groups of GMO molecules. Some of the defects observed over the course of the simulations were quite deep, reaching almost half the average width of the bilayer for an atomic-sized probe. Such thinning defects might provide effective pathways for unassisted transport of ions. This view is supported by measurements which show that permeability of homogeneous membranes to these solutes is significantly larger than would be anticipated assuming a constant average thickness of the bilayer.[11,12]

Defects in the surface of the bilayer are partially penetrated by water molecules. This is suggested by significant overlap between density profiles of water and head groups and is further confirmed by oxygen–oxygen radial distribution functions between water and GMO head groups. The observed molecular-scale water penetration into the head group region of the bilayer is in contrast with the results for interfaces between water and nonpolar liquids[39,40] where no appreciable mixing between the two components was found. In line with this conclusion, water penetration into the hydrocarbon core of the GMO bilayer was found to be quite small.

The structure of the water near the bilayer has been examined and compared with the structure of the liquid–vapor interface. In both cases, the most probable orientation of dipole moments of the interfacial water molecules is parallel to the interface and the net excess dipole moment of the interface points into the aqueous phase. There is, however, evidence that the hydrophilic surface presented by the bilayer disrupts the aqueous interface. In particular, water polarization along the interface normal exhibits non-monotonous behavior and the distribution of OH bond vectors is affected by hydrogen bonding of water molecules to the GMO head groups.

The interfacial dipole density generates a surface potential across the water–bilayer interface. The sign of the surface potential agrees with experimental results on GMO monolayers but its value is much larger than observed experimentally. One possible source of this discrepancy could be the neglect of intramolecular polarizability of the water molecules and the head groups in our potential energy function. This problem arises, to some extent, in a much simpler anisotropic system of the liquid–vapor interface of water. While the calculated structural properties of the interfacial water are in very good agreement with experimental results, the surface tension of water obtained from the TIP4P model is markedly underestimated.[62] The difficulty in accurate treatment of surface tension with pairwise additive potentials appears to be of a general nature—it was noted for another model of water,[50a] methanol,[63] and methyl chloride.[64] An additional source of errors can arise from truncating long-range interactions. In fact, proper treatment of polarization and long-range effects is probably the most important methodological issue in computer simulations of aqueous interfaces which still remains unresolved.

The surface potential is responsible, at least in part, for the existence of interfacial minima in the free energy of transfer of some small, polar solutes across membranes or liquid–liquid interfaces between water and nonpolar solvents.[65] This results in an apparent "interfacial resistance" to the transport of these solutes. Solute molecules experiencing such a resistance diffuse across the interfacial region much slower than anticipated from the conventional solubility-diffusion model which assumes that barriers for membrane entry and exit are negligible. In general, various structural characteristics of membranes, including nonuniform atomic density across the bilayer and formation of transient thinning defects, directly influence membrane phenomena such as transport across and interactions with the membrane of metabolites, drugs, anesthetics, neurotransmitters, small peptides, etc. This structure–function relationship is a subject of our current studies.

Acknowledgment. This work was supported by a grant from the NASA Exobiology Program through NASA-Ames–U.C. Santa Cruz Joint Research Interchange No. NCA 2-604 and NASA-Ames–U.C. San Francisco Cooperative Agreement No. NCC 2-772. Computer resources for this work were provided in part by the Numerical Aerodynamics Simulator (NAS) Program and by the National Cancer Institute Supercomputer Center.

(62) See ref 32—Section 3 for a review of computational and experimental results on the structure of the liquid–vapor interface of water and Section 9 for a discussion of calculations of surface tension.

(63) Matsumoto, M.; Kataoka, Y. *J. Chem. Phys.* **1989**, *90*, 2398–2407.

(64) Amaral, L. A. M.; Cabral, B. J. *J. Phys.: Condens. Matter* **1993**, *5*, 1919–1934.

(65) Wilson, M. A.; Pohorille, A. In *Proceedings of the 26th Jerusalem Symposium on Quantum Chemistry and Biochemistry*; Levine, R., Pullman, B., and Jortner, J., Eds.; Kluwer: Dordrecht, 1993; in press.